






PI Controller for IPMC Actuators Based on Nafion®/PT Using Machine Vision for Feedback Response at Different Relative Humidities

Ariel Gustavo Zuquello^{a*} , Matheus Colovati Saccardo^b , Roger Gonçalves^b ,
Kaique Afonso Tozzi^c , Rafael Barbosa^d, Laos Alexandre Hirano^e, Carlos Henrique Scuracchio^b 

^aUniversidade Comunitária da Região de Chapecó, Escola Politécnica, Chapecó, SC, Brasil.

^bUniversidade Federal de São Carlos, Programa de Pós-Graduação em Ciência e Engenharia de Materiais, Rod. Washington Luiz, Km 235, 13565-905, São Carlos, SP, Brasil.

^cUniversité Grenoble Alpes, Centre National de la Recherche Scientifique (CNRS), Laboratoire d'Electrochimie et de Physico-Chimie des Matériaux et des Interfaces (LEPMI), UMR5279, 38000, Grenoble, France.

^dInstituto Federal de Educação, Ciência e Tecnologia de São Paulo, Araraquara, SP, Brasil

^eUniversidade Federal de Alfenas, Instituto de Ciência e Tecnologia (ICT), Poços de Caldas, MG, Brasil.

Received: October 06, 2021; Revised: July 22, 2022; Accepted: August 02, 2022

Ionomeric Polymer-Metal Composites (IPMCs) are sandwich-like materials based in a polymeric membrane covered on both sides by metallic electrodes. Its operation mechanism consists of hydrated ions migration in response to an external electrical field generated between the electrodes, leading to a spatially nonuniform mass accumulation which causes the device to bend. Its performance as an actuator depends mainly on the environment's relative humidity and electrical stimuli. Consequently, IPMCs present variations in the electromechanical properties exhibiting nonlinearities and time-varying behaviors, limiting the major applications. For this reason, this paper investigated a PI controller performance to overcome these drawbacks and effectively control a Nafion-based IPMC-Li⁺ exposed to different relative humidities and electrical stimuli. The PI control system uses a camera with a machine vision application as a feedback sensor. Support instrumentation was developed to control the relative humidity, apply an electrical stimulus, and measure the electromechanical response. The pattern recognition algorithm implemented in the controller is efficient, with accuracy above 95%, making the feedback sensor reliable. Therefore, the PI controller was effective, stable, and capable of controlling and characterizing IPMC devices when relative humidity was above 60% at a low-frequency displacement and avoided the undesired back-relaxation phenomenon.

Keywords: IPMC, PI controller, Machine vision, Relative humidity, Camera.

1. Introduction

Ionomeric Polymer-Metal Composites (IPMCs) are smart and bio-inspired materials that can perform bending movements in response to an electrical stimulus¹. They are sandwich-type composites formed by an ionic conductive polymeric membrane between metallic electrodes (Figure 1a). The main characteristics are low density, noiselessness, miniaturization capacity, and biocompatibility². For this reason, they are promising materials for a wide range of technological applications in strategic areas, such as conductive rubber composites (CRC)³, actuators^{4,5}, sensors⁶⁻⁸, artificial muscles⁹, robotics^{10,11}, aerospace industry¹², energy harvesting¹³, biomimicry^{14,15}, and oil exploration¹⁶.

These devices' operating mechanism consists of hydrated ions migration inside the ionomeric channels in response to an electric field generated after a bias application in the metal electrodes¹⁷. This ionic movement causes an internal pressure

gradient, leading to a spatially nonuniform mass accumulation, which causes the device to bend¹⁸ (Figure 1b). Therefore, several factors influence mechanical performance, such as the dependence on the operating environment (temperature and humidity)¹⁹⁻²², counterion type²³, polymeric membrane dimensions (especially the thickness), and electrode physical properties²⁴.

The chemical structure of Nafion® consists of a polytetrafluoroethylene-like backbone (hydrophobic domain) with side-grafted chains containing sulfonic groups (hydrophilic domain), as seen in Figure 1c²⁵. Due to chemical incompatibility between these domains, the hydrophobic region is organized into an amorphous matrix with small crystalline domains, while the hydrophilic region coalesces, forming a three-dimensional network of channels (Figure 1d) called ionomeric channels²⁶. When the IPMC is exposed to an environment with high relative humidity, greater absorption of water molecules occurs through a first-order kinetic reaction (chemical reaction in which its speed linearly depends on

*e-mail: arielzuquello@gmail.com

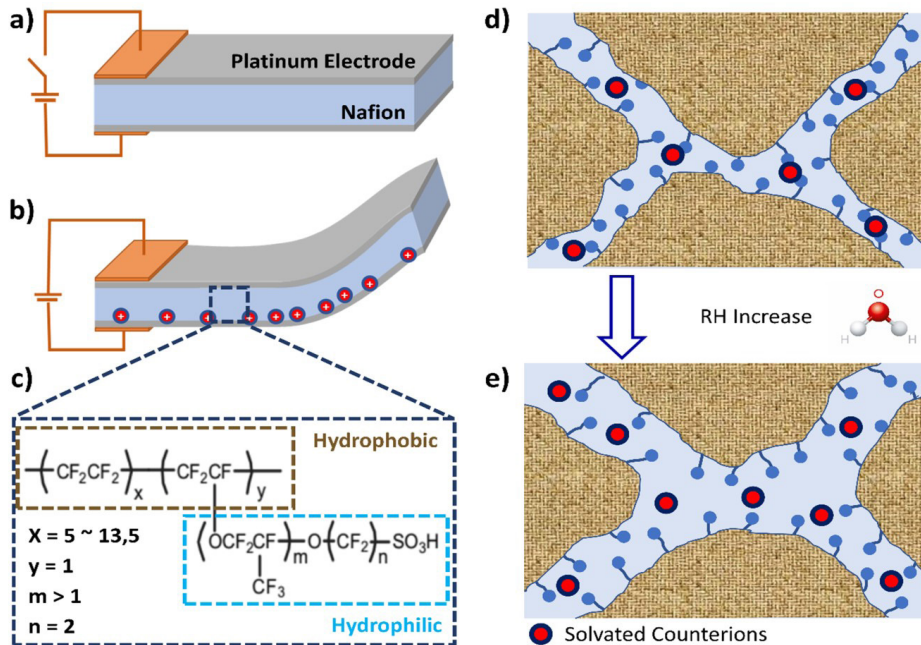


Figure 1. a) IPMC; b) IPMC mechanical response after a bias application; c) Nafion® chemical structure; d) hydrophilic domains at ambient humidity; e) hydrophilic domains at high humidity.

the concentration of the reactant), causing an expansion of the ionomeric channels. (Figure 1e)²⁷.

As this phenomenon depends on the environment's relative humidity in which the IPMC operates, its electromechanical response will be unpredictable in the absence of the control of this variable. Therefore, some studies present alternatives to prevent Nafion's hydration level variations during its operation. Among them is the use of non-aqueous solvent, as is the case of ionic liquid²⁸, the use of IPMC encapsulation²⁹, applications in an underwater environment, and applications in a controlled RH environment³⁰, which is the case of this paper.

Other phenomena are also observed, such as back-relaxation (drawback associated with water counter diffusion, which causes the IPMC to shift in the opposite direction after maintaining a bias for a while)^{23,31}, electrolysis (a reaction that splits water into hydrogen and oxygen)³², hysteresis (tendency to conserve their properties in the absence of the stimulus that generated them)³³, and highly uncertain³⁴. In other words, these devices have variations and instabilities in electromechanical performance, exhibiting nonlinearities and time-varying behaviors³⁵. For this reason, the IPMC has been coupled to a control system for robotic actuator applications³⁶, using techniques based on input/output response^{34,37-40}. Some authors have demonstrated the ability to effectively control robotic fingers⁴¹, soft robot⁴², artificial muscles^{43,44}, pneumatic muscle actuators⁴⁵, strain⁴⁶, force⁴⁷, position^{48,49}, and micropumps⁵⁰, using input/output controllers.

Although there are many types of controllers, PID (proportional–integral–derivative) controllers are the most common and versatile^{45,51}. Its operation consists of acquiring a signal, then computing the desired actuator output by calculating proportional, integral, and derivative responses and summing those three components to compute the output. Since the IPMC's operation and response frequency are low,

a PI controller is enough to ensure system functioning and reliability. These are simple, easy-to-understand, optimized control techniques with great popularity and are widely used in the industry⁵². In IPMC applications, the operation and response frequency is low. For this reason, a PI controller is enough to ensure system functioning and reliability.

Liao et al.⁵³ have proposed a PI robust tracking control design for an IPMC using an optimization coprime factorization approach to determine the PI controller parameter. Wang et al.⁵⁴ transformed simple and sophisticated PI control systems with machine vision as a feedback sensor. Liu et al.⁵⁵ developed an adaptive, nonlinear tuning algorithm to optimize the positional control of an IPMC actuated rotary mechanism using a PI controller. Fu et al.⁵⁶ created an IPMC robotic surgical device with a PI controller's embedded force feedback sensor.

In general, these controllers proved to be effective in ensuring proper system functioning and reliability. They can also precisely track position, eliminate steady-state errors, run effectively under a static or low-frequency operation, and have highly adjustable performance. However, there are always gaps for new adjustments like any method: i) Using a PI controller and a camera with a machine vision algorithm as feedback response. ii) Consider the instabilities caused by the external factors, such as relative humidity, that influence the IPMC mechanical response and, consequently, the controller's performance. iii) Verify the camera's tracking and monitoring capability and its influence on the system's ability to control the IPMC. Therefore, complementary studies combining methods focusing on the controller's performance under different operating conditions are desirable.

Thus, in this paper, a Nafion-based IPMC with platinum electrodes exchanged with Li⁺ ions was electromechanically controlled, employing a closed-loop PI system. A camera

and a machine vision application were used to track the tip displacement and provide feedback response. The system was considered a black-box model, samples were studied in a cantilever configuration, and the analyses were carried out using a humidity control system with precise RH control. Therefore, this paper aims to determine whether PI controllers using an image as a feedback response can competently control IPMC devices under varying relative humidity conditions and different types of the electrical stimulus.

2. Experimental

2.1. IPMC sample preparation

A Nafion-based IPMC with platinum electrodes was used in this paper. Nafion 117 (1100 equivalent weight, 178.0 μm thick) membranes were obtained from IonPower. The impregnation-reduction method described by Oguro et al.⁵⁷ was used to assemble these lithium ion-exchanged devices. This procedure aims to obtain IPMC samples with excellent quality and capable of mechanically responding to electrical stimuli.

2.2. Experimental setup

2.2.1. IPMC power source system

An electrical control system was developed to control the sample, using a current and voltage amplifier OPA551 (Buffer), a National Instruments (NI) electric signal generator NI-9263 module, and a data acquisition NI-9218 module. The NI-9263 signal is amplified by the OPA551 and electrically stimulates the IPMC. The NI-9218 module monitors the applied electric stimulus.

2.2.2. Instrumentation

Displacement measurements based on high-speed cameras are becoming a standard tool for interpreting IPMC deformation behavior⁵⁸⁻⁶¹. The technique showed an excellent performance in characterizing these materials. Moreover, it could be an alternative for IPMC actuator feedback control since it can track position with high speed and precision⁶². Also, it is an efficient, effective, and low-cost technique⁶³. For this reason, the IPMC control system used for feedback control was developed as described subsequently. Figure 2a

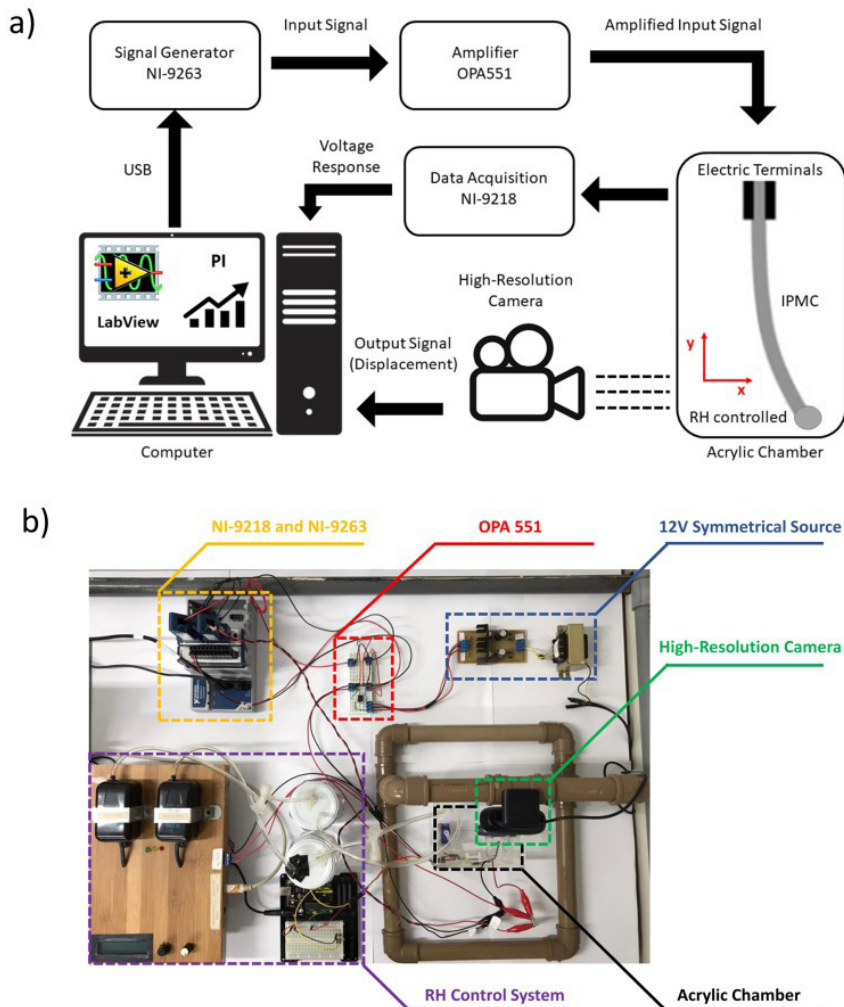


Figure 2. a) IPMC closed-loop control scheme and b) experimental setup.

presents the control system scheme, while Figure 2b shows the experimental setup.

The power source system and a high-resolution camera are connected and controlled by a computer (Laboratory Virtual Instrument Engineering Workbench - LabView). On the computer, a desired position value for the actuator is set. The power source system provides the electrical stimulus (input signal), allowing the actuator to bend. This movement (output signal) is real-time tracked by a low-cost and high-resolution camera CMOS (model Logitech c920), with a 30 frames/sec rate and a resolution of 1920 x 1080 pixels per frame processed by a machine vision application. The output signal provides a feedback response to the computer, calculated using a PI control, which monitors the electrical stimulus adjusting the input signal to obtain the desired device bending. A maximum voltage range of 2.0 V was used to maintain the device's integrity. The NI-9218 module acquires the IPMC voltage response.

PI is a practical, straightforward feedback control method specifying a process variable and set point. The PI controller was implemented using a LabView code block in the Control Design and Simulation/PID/PID.vi module. This module assists in dynamic systems simulation, controller designs, and real-time control systems. The process variable is the system parameter to be controlled (e.g., displacement), and the setpoint is the desired value for that system parameter. When the system is triggered, the PI controller determines a controller output value (e.g., electrical stimulus intensity) and applies the controller output value to the system to drive the process variable toward the setpoint value, controlling the IPMC displacement.

The PI control parameters (K_c - controller gain and T_i - reset Time (integral Time)) were tuned via the heuristic Ziegler-Nichols step response method since it is effortless and intuitively easy to understand. Tuning was performed for $RH = 90\%$. Since the main objective is to verify the influence of RH on the control system, the same tuning value was used for all RH tested.

2.2.3. Machine vision for feedback response

This study's visual inspection task is "Sorting" (searching for objects based on a template)⁶⁴. In this approach, the camera identifies patterns, quickly locating regions of the IPMC that match a known reference pattern (template).

When using pattern matching, it is created a template (w) that represents the searching object (IPMC tip) in a specific inspected image (C). Then, the machine vision application searches the template over Time, multiplying each pixel by the image pixel it overlaps. Summing the results over all the pixels of the template is possible to track the IPMC movement. In this paper, a normalized cross-correlation pattern matching algorithm was used. The image cross-correlation is defined according to Equation 1:

$$C(i, j) = \sum_{x=0}^{L-1} \sum_{y=1}^{K-1} w(x, y) f(x+i, y+j) \quad (1)$$

and normalized correlation as Equation 2:

$$R(i, j) = \frac{\sum_{x=0}^{L-1} \sum_{y=1}^{K-1} (w(x, y) - \bar{w}) (f(x+i, y+j) - \bar{f}(i, j))}{\left[\sum_{x=0}^{L-1} \sum_{y=1}^{K-1} (w(x, y) - \bar{w})^2 \right]^{1/2} \left[\sum_{x=0}^{L-1} \sum_{y=1}^{K-1} (f(x+i, y+j) - \bar{f}(i, j))^2 \right]^{1/2}} \quad (2)$$

where $w(x, y)$ is a pixel of the template, $f(i, j)$ is a pixel of the inspected image, \bar{w} and \bar{f} are intensity averages of template respectively image. Figure 3a shows the template (w) created in the inspected image (C). Figure 3b presents the visual inspection task when the IPMC is bending.

Equation 1 is a mathematical function that can inspect the entire reference image (C) and search the template (w) by sliding it on a pixel-by-pixel basis. As a summation, the function can scroll through the image from the upper left corner and advance to the next pixel, comparing the template's functions to the inspection image. The correlation coefficient is high when the function values are very similar; therefore, the template and the inspection image are equivalents. The normalized correlation (Equation 2) evaluates the degree of similarity between images. It is used because it is less sensitive to linear illumination changes, improving the template detection capacity. In equations, relative displacement is measured in pixels, a relative unit of measurement. For this reason, a reference with an object of known size was used to convert the pixel to mm, allowing the determination of the IPMC displacement in mm.

2.3. Experimental procedure

As described, IPMCs actuators and sensors are studied in a cantilever configuration, in which a bar-shaped structural

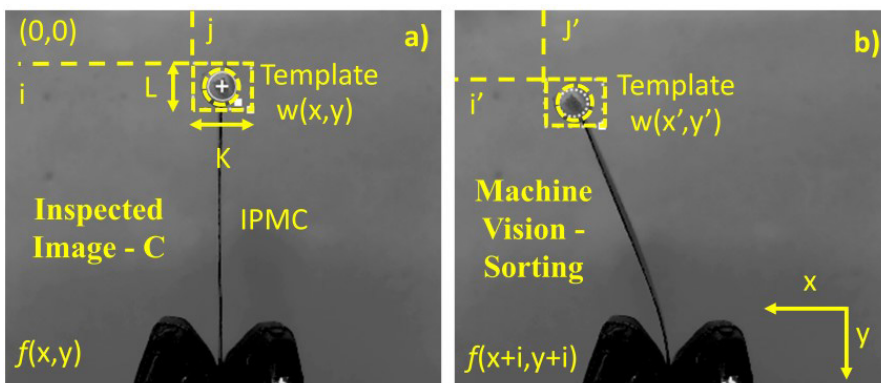


Figure 3. a) Template (w) created in the inspected image (C) and b) Visual inspection task.

element is anchored at one end. In contrast, the other end is free to move⁶⁵. This device’s electromechanical behavior depends on the environment’s relative humidity (RH) in which the sample is inserted. For this reason, this paper studied samples in a cantilever configuration (Figure 2). The analyses were carried out with precise RH control, using a humidity control system described in previous work¹⁷.

Therefore, to avoid any sample hydration level variation during the tests, the IPMC was kept in a closed chamber, controlling the RH continuously for 120 minutes to achieve osmotic equilibrium and kept constant until the end of test²³.

The experiments were carried out at RH = 30, 60, and 90% to investigate the PI controller performance under these conditions. After reaching the osmotic equilibrium, the desired displacement was adjusted manually in LabView. The power source system is automatically triggered, applying a voltage, causing the sample displacement. The movement response is tracked by the camera (installed along the axial direction of the actuator), giving a feedback real-time output signal at 30 fps. This captured signal is transmitted to a computer and used by a PI controller software that adjusts the voltage input signal to reach the previously adjusted displacement set point. All those components form a closed-loop control system represented in Figure 4.

3. Results and Discussions

3.1. Controller position tracking response

Path tracking experiments were conducted to verify the system’s ability to accurately and precisely follow a trajectory in real-time. In this analysis, RH = 90% was used since, in this condition, the device’s mechanical response is as fast as possible¹⁷, demanding maximum system performance. Figure 5a presents the IPMC displacement as a function of time. Problems were found in the initial tests, especially concerning the template search in the inspection image. It occurs because the template was created based on the tip of the IPMC (Figure 5b), and as it is a film, the side surface

area is small, making it difficult for the system to find the template in the inspected image. Therefore, it was decided to use a marker (small styrofoam ball) on the tip of the IPMC to maximize the recognition area and consequently improve the system accuracy (Figure 5c). This larger area improved the accuracy of the algorithm when recognizing the template.

Regarding the algorithm, it was necessary to use a marker to optimize its detection capacity. In Figure 5a, the recognition score represents the system’s accuracy in finding the model in the inspection image (secondary y-axis). The system used a minimum value for object recognition set at 70% (700 points from 0-1000). If the model found in the inspection image was $\geq 70\%$ similar to the first model image, the system could accurately track the IPMC movement. Otherwise, the system loses the model’s reference, and thus, it can no longer control it. When the Styrofoam ball was used, the score was higher than 95%, showing an excellent tracking ability. Then, it was decided to use the marking on the IPMC tip in all measurements.

Concerning the camera tracking capability, as soon as the control system was activated, the IPMC moved to the setpoint position. A few seconds later, the IPMC reached the determined displacement position when the setpoint was changed to force a new displacement. The maximum displacement achieved was 4.0 mm. No significant fluctuations were observed, even though the displacement was performed in the opposite direction. The camera was also able to track IPMC position with high speed and precision, giving feedback in real-time and high-quality signal to the PI system. The system, in turn, could adjust the electrical output signal quickly. For this reason, the device performed a predefined trajectory as desired.

Nemat-Nasser and Wu⁶⁶ studied with precision IPMCs high-frequency motion with a high-speed camera (120 frames/sec). On the other hand, Tsiakimakis et al.⁶⁰ used a CCD camera (30 frames/sec) to track with precision an IPMC movement at a low-frequency condition – 0.5 Hz. The authors affirm that monitoring problems may appear when high-frequency

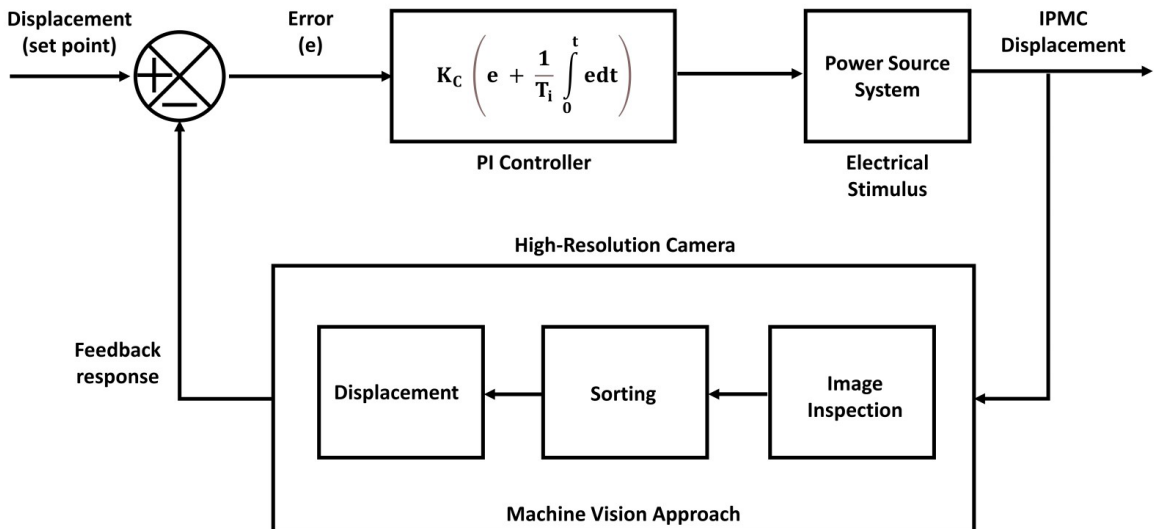


Figure 4. IPMC automatic closed-loop control system block diagram. The control parameters are Kc - controller gain and Ti - integral Time.

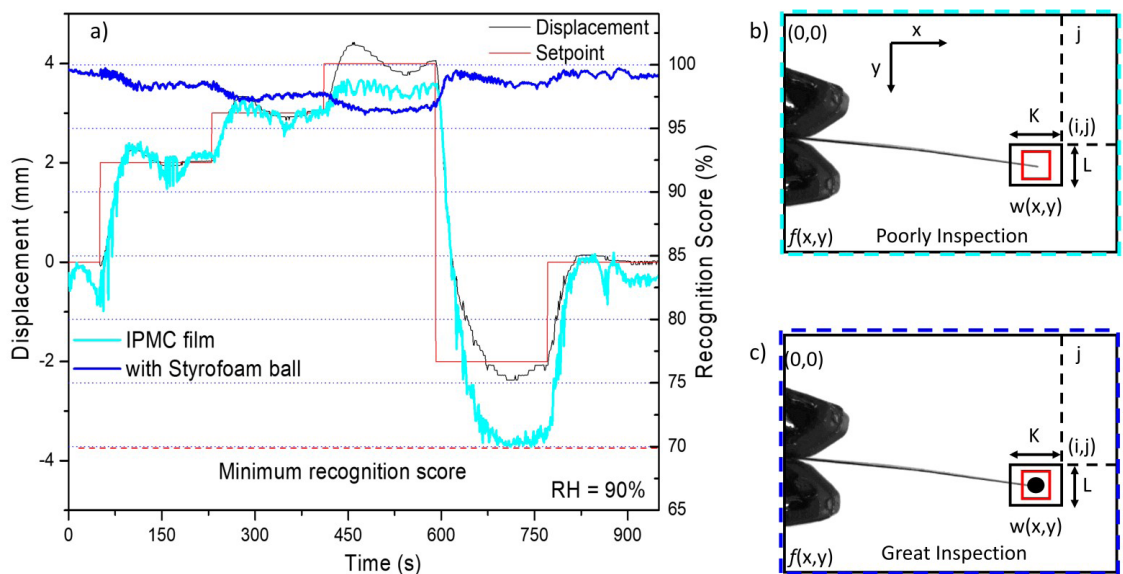


Figure 5. a) IPMC position tracking as a function of Time, b) IPMC film inspection, and c) IPMC film inspection using a small styrofoam ball marker.

movements are tracked by limited frame rate cameras (25–30 frames/sec). However, as noted in this work, the fast bending movement was accurately monitored, and system perturbations were not observed.

3.2. PI controller response

A high-precision control is necessary to operate and use an IPMC as a manipulation device (e.g., micro gripper)⁴¹. So, to verify the system's position tracking capacity as a function of the RH, the samples were tested under different non-sinusoidal waveform stimuli for RH = 30 ~ 90%. The PI controller was activated, electrically stimulating the IPMC. The high-resolution camera captured the displacement, while the NI-9218 module acquired the voltage and current responses.

3.2.1. Square step pulse

Figure 6 presents the IPMC displacement, voltage, and current responses as a function of Time for a square pulse stimulus (4.0 mm amplitude and 2.0 seconds interval).

As observed in Figure 6, as soon as the square pulse stimulus was applied, the IPMC moved toward the setpoint position. The displacement was more significant and faster when RH = 90% in both directions (Figure 6a). Besides, as the square pulse has a significant amplitude, the system applied the maximum allowable voltage (2.0 V) to reach the set point. As expected, after the pulse interval (2.0 seconds), the controller applied an opposite voltage to ensure that the IPMC returns to the initial position (0.0 mm) as soon as possible (Figure 6b). Regarding the IPMC current response, it is clear that the current peaked and then decreased exponentially as a function of time after applying the voltage. When RH > 60%, a second peak was observed, related to the voltage application in the opposite direction. On the other hand, the current remained constant when RH = 30% (Figure 6c).

When the controller triggers the IPMC device, the positively charged Li^+ ions complexed with water molecules migrate from the cathode to the anode, generating a current peak response⁶⁷. The ionic transport mechanisms are related to the actuator hydration level¹⁷. Saccardo et al.²³ analyzed the variation in the magnitude of the impedance ($|Z|$) as a function of RH using Impedance Spectroscopy. At low frequencies, it was observed that the ionic response of the material dominates it. Besides, as the hydration level increases, the amount of the H_2O molecule inside the membrane also increases, promoting a more significant ionic migration. For this reason, when RH > 60%, solvated ions can migrate in greater quantity and quickly, causing a more significant spatially nonuniform mass accumulation within the membrane and promoting a more substantial displacement.

Consequently, the electrical response was easily acquired when RH > 60%. Since, at this condition, even with a small voltage, the ionic mobility is high enough that Li^+ ions migrate quickly towards the anode, generating a peak current. With this, it is evident that the actuator presented an acceptable mechanical and electrical response for RH > 60% under a square pulse stimulus. The IPMC's operation and response frequency are low. So, evaluating the actuator response in these low-frequency conditions is essential to ascertain the controller efficiency.

3.2.2. Triangular wave

Figure 7 presents a bi-directional non-sinusoidal triangular waveform stimulus (4.0 mm amplitude and 2.0 seconds interval), in which the setpoint increased at a variable rate. The rate at which the setpoint changes between each ramp direction is equal during both cycle halves.

When the displacement rate (setpoint) was adjusted to 0.02 mm s^{-1} , the device presented an identical movement to the setpoint for all tested RH. The controller showed a quick

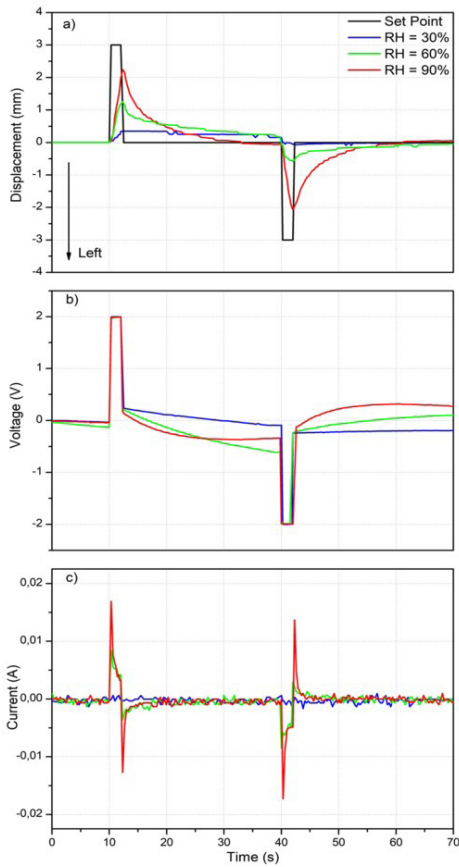


Figure 6. IPMC electromechanical response as a function of Time for a square pulse stimulus. a) Displacement (mm), b) Voltage (V), and c) Current (A).

response time and a small steady-state error at this condition. The PI control’s integral element can also slow the material relaxation when $RH > 60\%$, gradually increasing the applied voltage. On the other hand, the response is slower when the $RH = 30\%$, and the maximum voltage was used to ensure the proper movement. There is still reasonable trajectory control, increasing the displacement rate to 0.05 mm s^{-1} . The current response was as expected, following the behavior of the voltage.

Increasing the displacement rate requires a faster response from the actuator. Thus, when $RH = 90\%$, the controller can adequately control the sample for displacement rates up to 0.1 mm s^{-1} . Above this value, the IPMC displacement differs from the ideal. When the displacement rate is maximum (0.5 mm s^{-1}), the sample at $RH = 90\%$ could only reach half the setpoint, while the others did not present an adequate displacement. At this condition, the change in the setpoint is so fast that the controller cannot send the maximum possible voltage (2.0 V). As noted, the controller’s ability to manipulate the IPMC depends on environment RH and the displacement rate required. The PI controller performs satisfactorily when the $RH > 60\%$ and the displacement rate is less than 0.1 mm s^{-1} .

Once again, it is evident that controller efficiency is directly related to material characteristics and RH. Many different structural models have been proposed to explain Nafion’s morphology and properties⁶⁸⁻⁷¹. The most accepted²⁶ shows that increasing the H_2O absorption increases the average separation between ionic clusters, reducing Coulomb interactions between charged species (Li^+ and SO_3^- groups). So, at lower displacement rates and $RH > 60\%$, the counterion complexed with water molecules tends to easily migrate through the material to maintain the actuator position

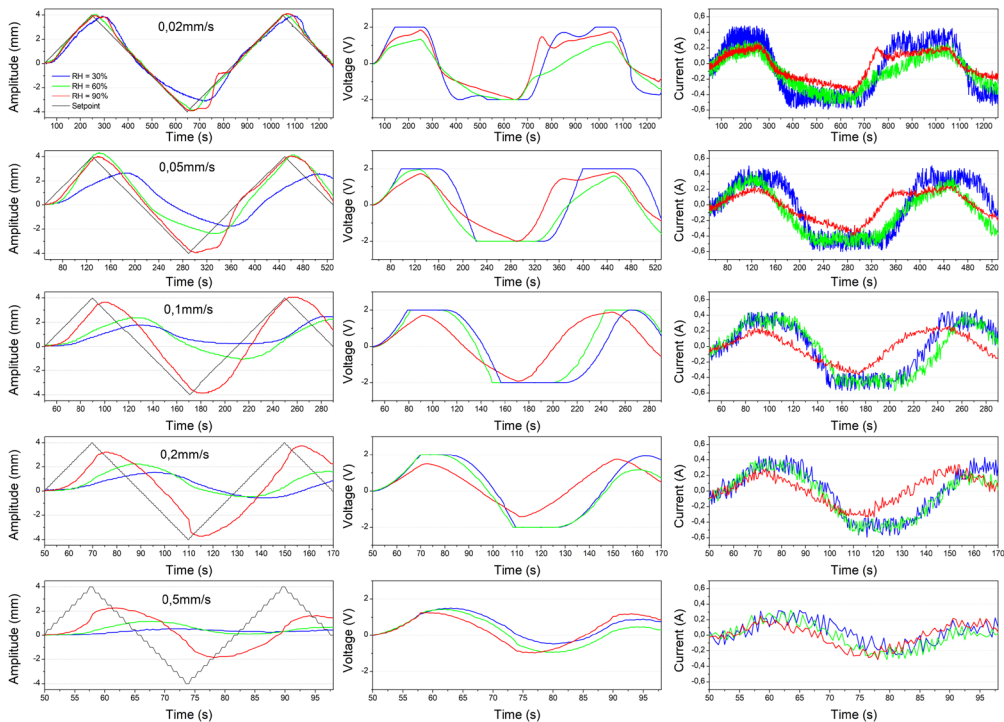


Figure 7. IPMC electromechanical response as a function of Time for a bi-directional non-sinusoidal triangular waveform stimulus.

relative to the setpoint. As the rate increases and $RH = 30\%$, the molecular motion is out of phase with the setpoint by a value proportional to the amount of water inside the IPMC, causing a slow trajectory adjustment.

3.2.3. Step response

The system maintains stability, even in disturbances or variations, ensuring reliability⁷². Thus, IPMC samples were submitted to a displacement for an extended period (300 seconds) to evaluate the system stability. The samples were studied under different displacement amplitudes (2.0, 3.0, and 5.0 mm), and $RH = 90\%$ was used since, in this environment condition, the device presents the highest possible deformation speed. Figure 8 illustrates the IPMC displacement as a function of time.

As soon as a voltage was applied, the IPMC moved to the setpoint position. The rise time (the Time it takes the system to go from 10% to 90% of the steady-state) was approximately 30 seconds, regardless of the set point. All samples showed overshoot, which increased as the displacement rose. However, the controller could correct this effect, reaching the desired position after a few seconds. The IPMC position varied less than 5% around the adjusted value, achieving its steady-state after 100 seconds (settling Time). The undesirable deadtime (how long it takes before a process begins to respond to a controller output change) was not observed. This behavior shows that both the output (displacement) and the input (voltage) signal were quickly monitored and adjusted, respectively, guarantying stability. So, the tracker system was designed able to achieve its primary task.

As shown previously, several papers have effectively controlled IPMCs using input/output controllers⁴²⁻⁴⁶. Many researchers have chosen a PI controller for its simplicity^{55,73-75}. Aw et al.⁷⁶ designed a PI controller to monitor a robotic surgical instrument with one skeleton-joint mechanism actuated by IPMC. The device operated as expected, providing various cutting forces with reasonable accuracy. Hunt et al.⁷⁷ presented an IPMC sensor-actuator camera-based feedback PI control.

They consider that the proposed setup could be usable with some improvements. Tondo et al.⁷⁸ demonstrated that a linear PI controller, including voltage constraints, is a simple and efficient approach for a bending actuator closed-loop control.

Generally, P and I are defined to obtain a closed control system with a minimum and constant steady-state. Therefore, the derivative term increases until the loop is acceptably fast concerning its set point. Increasing the derivative term decreases the overshoot, increases the gain, maintains stability, and makes the system highly sensitive to noise⁷². The response derivative can make the control system unstable if the control loop rate is too slow. Since the IPMCs device response is low frequency, D is unnecessary once overshooting is significant. For this reason, the proposed PI controller was effective and stable with values for the components $P = 0,01$ and $I = 0,04$ in our tests. Consequently, this system can control and characterize IPMC devices, as shown in the following section.

3.3. PI controller performance as a function of RH

As the actuator's mechanical performance is highly dependent on the operating environment RH (membrane hydration level)¹⁷, it is necessary to evaluate the ability to control and characterize IPMCs under different operating conditions to understand their behavior concerning these conditions. Then, all samples were previously tested at each RH to determine the maximum possible displacement. A state machine was then developed for each situation, allowing the maximum displacement to be varied every 300 seconds (3.3 mHz frequency). Besides, the electric drive system was limited to 2.0 V, ensuring the tested sample integrity. Displacement and voltage response as a function of Time were obtained when $RH = 30, 60$, and 90% , as shown in Figures 8a, 8b, and 8c, respectively.

As expected, the mechanical response is highly RH-dependent. By increasing the RH, the displacement amplitude becomes more accentuated and faster. When $RH = 30\%$, the

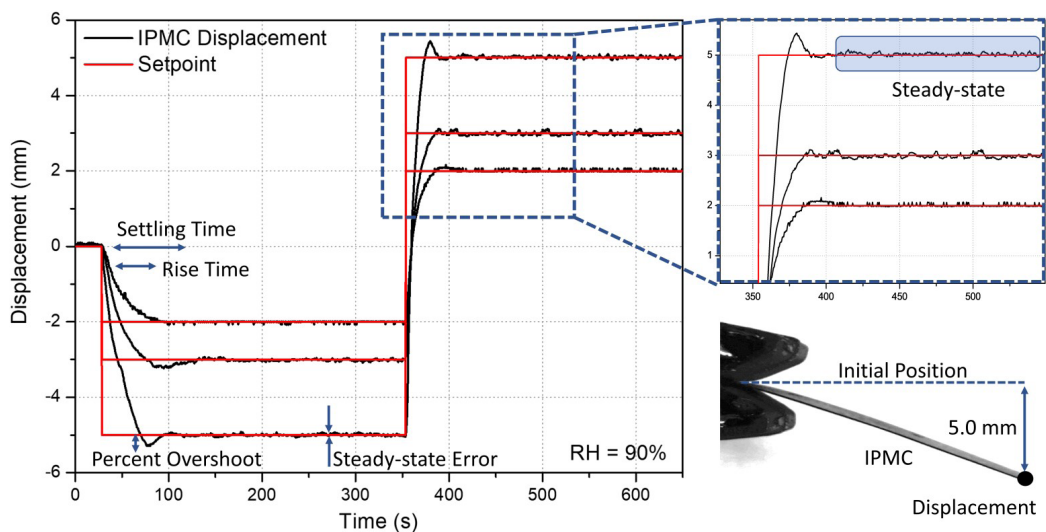


Figure 8. IPMC displacement as a function of Time showing the PI controller stability.

maximum displacement was 0.5 mm, whereas for RH = 90%, it was 5.0 mm. That is, the displacement increased ten times with a small membrane hydration level variation. The maximum displacement observed for RH = 60% was 3.0 mm, considerably higher than the driest condition tested. As shown elsewhere¹⁷, solvated ions can migrate/diffuse easily and in larger amounts inside the membrane when the RH = 90%. In addition, the more hydrated material favors displacement due to the reduction in the elastic modulus⁷⁹ Lei et al.¹⁹ determined from physical models that Young's modulus decreases with increasing RH. Likewise, Bernat and Kolota²¹ found that once the water content in the Nafion membrane increases, the flow dynamics increase significantly. For this reason, the speed and amplitude of the mechanical response vary significantly depending on the membrane's hydration level.

The highest overshooting sample was conditioned at RH = 30%. After reaching the maximum displacement value, the controller reduces the applied voltage to 0.0 V (Figure 9a). However, as the RH is very low, few H₂O molecules are inside the membrane³¹. Consequently, the ionic migration in the opposite direction is very slow, so the device takes a long time to return to the desired position. Despite the high-precision control, stability, and accuracy, the PI controller performed poorly under these conditions. A more accurate and faster response could be obtained for a broader voltage range (up to 5.0 V), but with the possible intensification of other phenomena, such as water electrolysis²⁸. Adding the derivative term to decrease the overshoot would also be possible, increasing the gain in exchange for the system instability risk.

The ionic migration is much easier and more intense when the RH > 90% (Figure 9c). Once it reached a displacement ten times greater, the controller reached voltages of ~1.25 V. On the other hand, the applied voltage gradually increased after reaching the desired displacement. This effect may be associated with back-relaxation⁸⁰. When an electrical stimulus is applied to the IPMC, ions solvated with water molecules migrate in the cathode direction. Instead of maintaining its deformation, the device decays back to its initial shape⁸¹. Therefore, the controller increases the electrical stimulus intensity to avoid this undesired phenomenon. Thus, the displacement kept the adjusted position over Time.

A complementary statistical analysis was performed for a 1.0 and 1.5 V voltage range. Table 1 summarizes the data obtained. R-squared (R²) represents the relationship between the setpoint and the process variable, showing how close the IPMC displacement is to the desired trajectory. The displacement depends on the voltage and RH. Therefore, for each condition, maximum displacement was adjusted. The overshoot percentage was calculated about this maximum displacement. The settling time was determined when the sample displacement varied less than 5% around the setpoint. The displacement speed was considered using the ratio between the total distance covered by the sample and a given time interval.

As noted, R² increases as a function of RH and electrical stimulus. However, this factor is more strongly influenced by the RH variation since, for the same environmental condition, when doubling the applied voltage value, R² increases little.

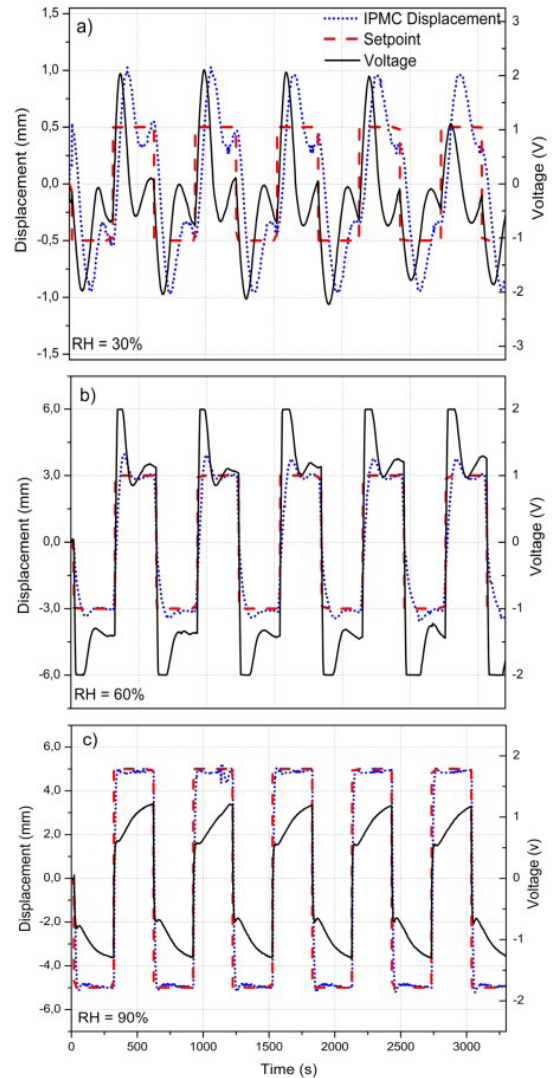


Figure 9. IPMC Displacement and voltage response as a function of time. a) RH = 30%, b) RH = 60%, and c) RH = 90%.

It shows that when the polymeric membrane hydration level is low, the IPMC control is difficult. The high overshoot value and the sample's observation did not reach the stabilization time during the experiment cycle interval (300 seconds). Moreover, when RH > 60%, the control was more effective, and both the overshoot and the stabilization time were acceptable and compatible with the expected.

The difference becomes even more significant when the displacement rate is analyzed individually. As can be observed, the sample with the highest hydration level showed a displacement rate 650 times higher than the sample conditioned in low RH. For this reason, the sample quickly reached the desired displacement, and, consequently, the stabilization time was obtained after a few seconds. Thus, it is clear that the IPMC's electromechanical performance is strongly influenced by the amount of H₂O molecules inside the Nafion's ionic channels. When the amount of H₂O is limited, the device's displacement is slight, and

Table 1. Device performance for various operating conditions, presenting R^2 , maximum displacement, overshoot percentage, settling Time, and displacement speed as a function of voltage range and RH.

RH (%)	Voltage Range (V)	R^2	Maximum Displacement (mm)	Overshoot Percentage (%)	Settling Time (s)	Displacement Rate (mm/s) (x10)
30	1.00	0.52	0.12	2.91	-	0.02
	1.50	0.56	0.24	15.81	-	0.03
	2.00	0.62	0.50	16.39	-	0.03
60	1.00	0.82	1.10	2.59	4.60	0.05
	1.50	0.84	2.08	4.73	9.20	0.2
	2.00	0.88	3.00	5.32	12.53	0.4
90	1.00	0.90	1.55	2.35	2.82	1.50
	1.50	0.92	3.06	4.62	6.80	17.30
	2.00	0.95	5.00	6.69	8.96	19.50

its control is compromised. In general, the IPMCs actuator's structure-properties relationship determines the efficiency of the PI controller. Variations arise since structural changes occur in the polymeric membrane for different RH, affecting the ion migration capacity. Thus, the variation of the electromechanical response of IPMC devices determined the efficiency of the PI controller.

4. Conclusion

In this paper, a closed-loop PI control system was developed to control a Nafion-based IPMC with platinum electrodes exchanged with Li^+ ions. The PI controller was chosen because it is widely used in the industry and is facile to understand and optimize.

Since the IPMCs operation and frequency response are low (overshooting is not great), the derivative action is unnecessary, and a PI controller could control the IPMC properly. The machine vision approach presented excellent accuracy when a marking on the tip of the IPMC was used since it increased the recognition area of the algorithm. It showed an excellent success rate ($> 95\%$) in object recognition in real-time concerning the model created by the algorithm. In general, the proposed system was effective, stable, and capable of controlling and characterizing IPMC devices.

The controller's performance was evaluated testing the IPMC device under different operating conditions, specifically varying the RH and the electrical stimuli. It was observed that the mechanical response is highly RH and bias dependent. However, it was evident that the hydration level is the most decisive factor in IPMCs' electromechanical behavior. When $\text{RH} \geq 60\%$, the device's mechanical performance was satisfactory, evidenced by the increase of the three parameters: coefficient of determination (R^2), displacement rate and tip displacement as a function of the three voltages evaluated. In other hands, in lower RH the observed parameters were reduced. This proves that dried environments mitigates the ionic mobility due to the smaller amount of solvated water molecules, reducing the ionomeric channels to the point of compromising the mechanical performance of the device.

In favorable environments ($\text{RH} \geq 60\%$), the PI controller avoided the undesired back-relaxation phenomenon, adjusting the electrical stimulus intensity over time. So, the actuator maintained its displacement during the experiment time. New experiments will improve control techniques and

explore others IPMC actuator variables (thickness, length, and width). Also, different solvents (non-aqueous), alkali metals counterions (H^+ , Na^+ , K^+) and ionic liquid (BMIM^+) will be used to study their influence on the IPMC performance and control.

5. Acknowledgments

This study was financed in part by the Coordenação de Aperfeiçoamento de Pessoal de Nível Superior (CAPES) - Finance Code 001. To CAPES for the scholarships process #88887.501393/2020-00, CAPES/DINTER - process #23038.021524/2016-88, CAPES/PROEX - process #88887.335799/2019-00, and CAPES/PRINT - process #88887.569936/2020-00. The authors would also like to thank the Fundação de Amparo à Pesquisa do Estado de São Paulo (FAPESP) - process #2018/07001-6, #2018/10843-9, #2018/09761-8, and #2020/02696-6.

6. References

- Bahramzadeh Y, Shahinpoor M. A review of ionic polymeric soft actuators and sensors. *Soft Robot.* 2014;1(1):38-52.
- Shahinpoor M. *Ionic Polymer Metal Composites (IPMCs): Smart Multi-Functional Materials and Artificial Muscles*. Vol. 2. London: Royal Society of Chemistry; 2015.
- Barbosa R, Gonçalves R, Tozzi KA, Saccardo MC, Zuquello AG, Scuracchio CH. Improving the swelling, mechanical, and electrical properties in natural rubber latex/carbon nanotubes nanocomposites: effect of the sonication method. *J Appl Polym Sci.* 2022;139(23):52325.
- Chen D, Pei Q. Electronic muscles and skins: a review of soft sensors and actuators. *Chem Rev.* 2017;117(17):11239-68.
- Kim KJ, Palmre V, Stalbaum T, Hwang T, Shen Q, Trabia S. Promising developments in marine applications with artificial muscles: electrodeless artificial cilia microfibers. *Mar Technol Soc J.* 2016;50(5):24-34.
- Palmre V, Pugal D, Kim KJ, Leang KK, Asaka K, Aabloo A. Nanothorn electrodes for ionic polymer-metal composite artificial muscles. *Sci Rep.* 2014;4:1-10.
- Kaasik F, Must I, Baranova I, Pöldsalu I, Lust E, Johanson U, et al. Scalable fabrication of ionic and capacitive laminate actuators for soft robotics. *Sens Actuators B Chem.* 2017;246:154-63.
- Fallahi A, Bahramzadeh Y, Tabatabaie SE, Shahinpoor M. A novel multifunctional soft robotic transducer made with poly (ethylene-co-methacrylic acid) ionomer metal nanocomposite. *Int J Intell Robot Appl.* 2017;1(2):143-56.

9. Ruiz S, Mead B, Palmre V, Kim KJ, Yim W. A cylindrical ionic polymer-metal composite-based robotic catheter platform: modeling, design and control. *Smart Mater Struct.* 2015;24(1):015007.
10. Aw KC, McDaid AJ. Bio-applications of ionic polymer metal composite transducers. *Smart Mater Struct.* 2014;23(7):074005.
11. Zolfagharian A, Kouzani AZ, Khoo SY, Moghadam AAA, Gibson I, Kaynak A. Evolution of 3D printed soft actuators. *Sens Actuators A Phys.* 2016;250:258-72.
12. Monzon A, Chow T, Guthrie P, Lu Z, Chuma C, He H, et al. Methods for promoting knowledge exchange and networking among young professionals in the aerospace sector - IAFs IPMC workshop 2013 insights. *Acta Astronaut.* 2016;118:123-9.
13. Patel SN, Mukherjee S. Shoe-based energy harvesting using ionic polymer metal composites. In: Kumar R, Chauhan VS, Talha M, Pathak H, editors. *Machines, mechanism and robotics. lecture notes in mechanical engineering.* Singapore: Springer; 2022. p. 169-77. https://doi.org/10.1007/978-981-16-0550-5_15.
14. Chu W-S, Lee K-T, Song S-H, Han M-W, Lee J-Y, Kim H-S, et al. Review of biomimetic underwater robots using smart actuators. *Int J Precis Eng Manuf.* 2012;13(7):1281-92.
15. Sfakiotakis M, Kazakidi A, Tsakiris DP. Octopus-inspired multi-arm robotic swimming. *Bioinspir Biomim.* 2015;10(3):035005.
16. Hu Q, Xu L, Liu X. MOGA application feasibility research on ocean petroleum exploration platform seawater environment supervision. In: 6th International Conference on Natural Computation, ICNC 2010; 2010; Yantai, China. *Proceedings. USA: IEEE;* 2010. p. 3503-7.
17. Saccardo MC, Zuquello AG, Tozzi KA, Gonçalves R, Hirano LA, Scuracchio CH. Counter-ion and humidity effects on electromechanical properties of Nafion®/Pt composites. *Mater Chem Phys.* 2020;244:122674. <http://dx.doi.org/10.1016/j.materchemphys.2020.122674>.
18. Drozdov AD. Modeling the response of polymer-ionic liquid electromechanical actuators. *Acta Mech.* 2016;227(2):437-65.
19. Lei H, Lim C, Tan X. Humidity-dependence of IPMC sensing dynamics: characterization and modeling from a physical perspective. *Meccanica.* 2015;50(11):2663-73.
20. Feng GH, Huang WL. Investigation on the mechanical and electrical behavior of a tuning fork-shaped ionic polymer metal composite actuator with a continuous water supply mechanism. *Sensors (Basel).* 2016;16(4):1-18.
21. Bernat J, Kolota J. Adaptive observer-based control for an IPMC actuator under varying humidity conditions. *Smart Mater Struct.* 2018;27(5):055004.
22. Aabloo A, Belikov J, Kaparin V, Kotta U. Challenges and perspectives in control of ionic Polymer-Metal Composite (IPMC) Actuators: A Survey. *IEEE Access.* 2020;8:121059-73.
23. Saccardo MC, Zuquello AG, Gonçalves R, Tozzi KA, Barbosa R, Hirano LA, et al. Electromechanical evaluation of ionomeric polymer-metal composites using video analysis. *Mater Res.* 2021;24(suppl 2):e20210317.
24. Kim H, Cha Y, Porfiri M. Voltage attenuation along the electrodes of ionic polymer metal composites. *J Intell Mater Syst Struct.* 2016;27(17):2426-30.
25. Mauritz KA, Moore RB. State of understanding of nafion. *Chem Rev.* 2004;104(10):4535-86.
26. Elliott JA, Wu D, Paddison SJ, Moore RB. A unified morphological description of Nafion membranes from SAXS and mesoscale simulations. *Soft Matter.* 2011;7(15):6820-7.
27. Gebel G. Structural evolution of water swollen perfluorosulfonated ionomers from dry membrane to solution. *Polymer (Guildf).* 2000;41(15):5829-38.
28. Gonçalves R, Tozzi KA, Saccardo MC, Zuquello AG, Scuracchio CH. Nafion-based ionomeric polymer/metal composites operating in the air: theoretical and electrochemical analysis. *J Solid State Electrochem.* 2020;24(8):1845-56.
29. Lei H, Li W, Tan X. Encapsulation of ionic polymer-metal composite (IPMC) sensors with thick parylene: fabrication process and characterization results. *Sens Actuators A Phys.* 2014;217:1-12.
30. Guo S, Shi L. IPMC actuator-based multifunctional underwater microrobots. In: Asaka K, Okuzaki H, editors. *Soft actuators materials, modeling, applications, and future perspectives.* Singapore: Springer; 2014.
31. Hirano LA, Acerbi LW, Kikuchi K, Tsuchitani S, Scuracchio CH. Study of the influence of the hydration level on the electromechanical behavior of nafion based ionomeric polymer-metal composites actuators. *Mater Res J Mater.* 2015;18(suppl 2):154-8.
32. Taghavi S, Mohammadi F, Barzin J. Ionic Polymer-Metal Composites (IPMC) from recycled Flemion(r) membrane used in chlor-alkali industry. *Sci Iran.* 2016;23:1117-28.
33. Shahinpoor M. *Ionic Polymer Metal Composites (IPMCs): smart multi-functional materials and artificial muscles.* Vol. 2. London: Royal Society of Chemistry; 2015.
34. Porfiri M, Sharghi H, Zhang P. Modeling back-relaxation in ionic polymer metal composites: the role of steric effects and composite layers. *J Appl Phys.* 2018;123(1):014901.
35. Moeinkhah H, Rezaeepazhand J, Akbarzadeh A. Analytical dynamic modeling of a cantilever IPMC actuator based on a distributed electrical circuit. *Smart Mater Struct.* 2013;22(5):055033.
36. McDaid AJ, Aw KC, Xie SQ, Haemmerle E. Gain scheduled control of IPMC actuators with 'model-free' iterative feedback tuning. *Sens Actuators A Phys.* 2010;164(1-2):137-47.
37. Bonomo C, Fortuna L, Giannone P, Graziani S, Strazzeri S. A model for ionic polymer metal composites as sensors. *Smart Mater Struct.* 2006;15(3):749-58.
38. La HM, Sheng W. Robust adaptive control with leakage modification for a nonlinear model of Ionic Polymer Metal Composites (IPMC). In: 2008 IEEE International Conference on Robotics and Biomimetics; 2009; Bangkok, Thailand. *Proceedings. USA: IEEE;* 2009. p. 1783-88. <http://dx.doi.org/10.1109/ROBIO.2009.4913272>.
39. Shi L, Guo S, Asaka K. Modeling and experiments of IPMC actuators for the position precision of underwater legged microrobots. In 2012 IEEE International Conference on Automation and Logistics; 2012; Zhengzhou, China. *Proceedings. USA: IEEE;* 2012. p. 415-20. <http://dx.doi.org/10.1109/ICAL.2012.6308244>.
40. Richardson RC, Levesley MC, Brown MD, Hawkes JA, Watterson K, Walker PG. Control of ionic polymer metal composites. *IEEE/ASME Trans Mechatron.* 2003;8(2):245-53.
41. Gonzalez C, Lumia R. An IPMC microgripper with integrated actuator and sensing for constant finger-tip displacement. *Smart Mater Struct.* 2015;24(5):055011.
42. Marchese AD, Komorowski K, Onal CD, Rus D. Design and control of a soft and continuously deformable 2D robotic manipulation system. In *Proceedings - IEEE International Conference on Robotics and Automation; 2014; Hong Kong, China. Proceedings. USA: IEEE;* 2014. p. 2189-96. <http://dx.doi.org/10.1109/ICRA.2014.6907161>.
43. Kaneda Y, Kamamichi N, Yamakita M, Asaka K, Luo ZW. Control of linear artificial muscle actuator using IPMC. In *SICE 2003 Annual Conference (IEEE Cat. No.03TH8734); 2003; Fukui, Japan. Proceedings. USA: IEEE;* 2003. p. 1650-5.
44. Lee MJ, Jung SH, Lee S, Mun MS, Moon I. Control of IPMC-based artificial muscle for myoelectric hand prosthesis. In: *The First IEEE/RAS-EMBS International Conference on Biomedical Robotics and Biomechatronics, 2006. BioRob 2006; 2006; Pisa. Proceedings. USA: IEEE;* 2006. p. 1172-7.
45. Andrikopoulos G, Nikolakopoulos G, Manesis S. Advanced nonlinear PID-based antagonistic control for pneumatic muscle actuators. *IEEE Trans Ind Electron.* 2014;61(12):6926-37.
46. Sutton L, Moein H, Rafiee A, Madden JDW, Menon C. Design of an assistive wrist orthosis using conductive nylon actuators.

- In: 6th IEEE International Conference on Biomedical Robotics and Biomechanics (BioRob); 2016; Singapore. Proceedings. USA: IEEE; 2016. p. 1074-9.
47. Sano S, Takagi K, Sato S, Hirayama S, Uchiyama N, Asaka K. Robust PID force control of IPMC actuators. *Proc SPIE*. 2010;17642.
 48. Bhat ND, Kim WJ. Precision position control of ionic polymer metal composite. *Proc Am Control Conf*. 2004;1:740-5.
 49. Kothera CS, Leo DJ. Position control of a square-plate ionic polymer actuator using output feedback. *J Intell Mater Syst Struct*. 2007;18(3):219-34.
 50. Yu W. The development of an IPMC actuated micropump using pid control with iterative feedback tuning [thesis]. Nova Zelândia: University of Auckland; 2011.
 51. Xu Y, Zhou J, Xue X, Fu W, Zhu W, Li C. An adaptively fast fuzzy fractional order PID control for pumped storage hydro unit using improved gravitational search algorithm. *Energy Convers Manage*. 2016;111:67-78.
 52. Cheon, K., Kim, J., Hamadache, M. & Lee, D. On replacing PID controller with deep learning controller for DC motor system. *J Autom Control Eng*. 2015;3(6):452-6. <http://dx.doi.org/10.12720/joace.3.6.452-456>.
 53. Liao W, Yan T, Wang A, Fu Y. IPMC robust nonlinear tracking control design based on a multi-objective particle swarm optimization-based RRCF approach. In: *International Conference on Advanced Mechatronic Systems (ICAMEchS)*; 2015; Beijing, China. Proceedings. USA: IEEE; 2015. p. 571-6. <http://dx.doi.org/10.1109/ICAMEchS.2015.7287176>.
 54. Wang X, Wang L, Guo S, Mills JK. A test-bed for visual servo control of artificial muscle micro-robot with parallel architecture. In: *2006 International Conference on Mechatronics and Automation*; 2006; Luoyang, China. Proceedings. USA: IEEE; 2006. p. 848-53. <http://dx.doi.org/10.1109/ICMA.2006.257720>.
 55. Liu D, McDaid AJ, Aw KC, Xie SQ. Position control of an ionic polymer metal composite actuated rotary joint using iterative feedback tuning. *Mechatronics*. 2011;21(1):315-28.
 56. Fu L, McDaid AJ, Aw KC. Control of an IPMC actuated robotic surgical tool with embedded interaction sensing. In *2013 IEEE/ASME International Conference on Advanced Intelligent Mechatronics*; 2013; Wollongong, NSW, Australia. Proceedings. USA: IEEE; 2013. p. 1255-9. <http://dx.doi.org/10.1109/AIM.2013.6584266>.
 57. Oguro K, Asaka K, Fujiwara N, Onishi K, Sewa S. Polymer electrolyte actuator driven by low voltage. *MRS Proc*. 1999;600:229.
 58. Bar-Cohen Y, Sherrit S, Lih SS. Characterization of the electromechanical properties of EAP materials. *Proc SPIE*. 2001;4329:319-27.
 59. Tsiakmakis K, Laopoulos T. Image analysis for measuring motion parameters with a CCD camera. In *2007 IEEE International Workshop on Imaging Systems and Techniques*; 2007; Cracovia, Poland. Proceedings. USA: IEEE; 2007. <http://dx.doi.org/10.1109/ist.2007.379606>.
 60. Tsiakmakis K, Brufau J, Puig-Vidal M, Laopoulos T. Measuring motion parameters of ionic polymer-metal composites (IPMC) actuators with a CCD camera. In: *2007 IEEE Instrumentation & Measurement Technology Conference IMTC 2007*; 2007; Warsaw, Poland. Proceedings. USA: IEEE; 2007. <http://dx.doi.org/10.1109/imtc.2007.379334>.
 61. Tsiakmakis K, Brufau-Penella J, Puig-Vidal M, Laopoulos T. A camera based method for the measurement of motion parameters of IPMC actuators. *IEEE Trans Instrum Meas*. 2009;58(8):2626-33.
 62. Kamamichi N, Takagi K, Sano S. Modeling and feedback control of electro-active polymer actuators. In: Asaka K, Okuzaki H, editors. *Soft actuators*. Tokyo: Springer; 2014. p. 327-41. https://doi.org/10.1007/978-4-431-54767-9_24.
 63. Tsiakmakis K, Laopoulos T. An improved tracking technique for visual measurements of ionic polymer-metal composites (IPMC) actuators using Compute Unified Device Architecture (CUDA). *Meas Sci Technol*. 2011;22(11):114006.
 64. Koniar D, Hargas L, Simonova A, Hrianka M, Loncova Z. Virtual instrumentation for visual inspection in mechatronic applications. *Procedia Eng*. 2014;96:227-34.
 65. Vokoun D, He Q, Heller L, Yu M, Dai Z. Modeling of IPMC Cantilever's displacements and blocking forces. *J Bionics Eng*. 2015;12(1):142-51.
 66. Nemat-Nasser S, Wu Y. Comparative experimental study of ionic polymer-metal composites with different backbone ionomers and in various cation forms. *J Appl Phys*. 2003;93(9):5255-67.
 67. Park J, Palmre V, Hwang T, Kim K, Yim W, Bae C. Electromechanical performance and other characteristics of IPMCs fabricated with various commercially available ion exchange membranes. *Smart Mater Struct*. 2014;23(7):074001.
 68. Gierke TD, Munn GE, Wilson FC. The morphology in nafion perfluorinated membrane products, as determined by wide- and small-angle x-ray studies. *J Polym Sci Part A-2, Polym Phys*. 1981;19(11):1687-704.
 69. Hsu WY, Gierke TD. Ion transport and clustering in nafion perfluorinated membranes. *J Membr Sci*. 1983;13(3):307-26.
 70. Fujimura M, Hashimoto T, Kawai H. Small-angle X-ray scattering study of perfluorinated ionomer membranes. 2. models for ionic scattering maximum. *Macromolecules*. 1982;15(1):136-44.
 71. Schmidt-Rohr K, Chen Q. Parallel cylindrical water nanochannels in Nafion fuel-cell membranes. *Nat Mater*. 2008;7(1):75-83.
 72. Goodwin GC, Graebe SF, Salgado ME. *Control system design*. Hoboken: Prentice Hall; 2000. p. 157-73.
 73. Al-Allaq A, Ansaf B, Jaksic N, Depalma JL. Modified nernst-plank-poisson model & control for IPMC with NI-ELVIS II. *J Eng Sci*. 2020. Preprints.
 74. Hunt A, Chen Z, Tan X, Kruusmaa M. An integrated electroactive polymer sensor – actuator : design, model-based control, and performance characterization. *Smart Mater Struct*. 2016;25(3):035016.
 75. Mead B, Ruiz S, Yim W. Closed-loop control of a tube-type cylindrical IPMC. *Proc SPIE - The Int Soc Optical Eng*, 2013;8687:86872Q.
 76. Aw K, Fu L, McDaid A. An IPMC actuated robotic surgery end effector with force sensing. *Int J Smart Nano Mater*. 2013;4(4):246-56.
 77. Hunt A, Chen Z, Tan X, Kruusmaa M. Feedback control of acoupled IPMC (Ionic Polymer-Metal Composite) sensor-actuator. In: *ASME Dynamic Systems and Control Conference 2009, DSCC2009*; 2009 Oct 12-14; Hollywood, California, USA. Proceedings. New York: ASME; 2010. p. 485-91. <http://dx.doi.org/10.1115/DSCC2009-2700>.
 78. Tondou B, Simaite A, Hari Shankar Lal Das GK, Soueres P, Bergaud C. Efficient linear approach for the closed-loop control of a ionic polymer bending actuator. *Adv. Sci. Technol*. 2016;97:75-80.
 79. Brunetto P, Fortuna L, Giannone P, Graziani S, Strazzeri S. Static and dynamic characterization of the temperature and humidity influence on IPMC actuators. *IEEE Trans Instrum Meas*. 2010;59(4):893-908.
 80. Porfiri M, Leronna A, Bardella L. An alternative explanation of back-relaxation in ionic polymer metal composites. *Extreme Mech Lett*. 2017;13:78-83.
 81. Vunder V, Punning A, Aabloo, A. Back-relaxation of carbon-based ionic electroactive polymer actuators. In: *ASME 2012 Conference on Smart Materials, Adaptive Structures and Intelligent Systems*; 2012 Sep 19-21; Stone Mountain, Georgia, USA. Proceedings. New York: ASME; 2012. p. 163-8. Vol. 1: *Development and Characterization of Multifunctional Materials; Modeling, Simulation and Control of Adaptive Systems; Structural Health Monitoring*. <http://dx.doi.org/10.1115/SMASIS2012-8127>.